Determination of Spacecraft Landing Footprint for Safe Planetary Landing

SCOTT R. PLOEN
HOMAYOUN SERAJI
CHARLES E. KINNEY
NASA Jet Propulsion Laboratory

A methodology is developed based on a ballistic analysis to estimate the landing footprint associated with the powered terminal descent phase of a spacecraft soft landing. The analysis is based on an idealized two-impulse thrust maneuver and leads to an analytical expression for the elliptical boundary of the landing footprint. The objective is to develop a computationally efficient method to estimate the landing footprint for use in an on-board fuzzy-logic based inference engine for real-time hazard avoidance. The inference engine combines an estimate of the landing footprint with information about the safeness of the landing terrain to construct an overall landing site quality index. The landing site quality index is a critical parameter that enables the spacecraft to make intelligent real-time decisions about landing safely on unknown and hazardous terrains. The footprint generated from the ballistic analysis is also compared with the footprint resulting from numerically integrating a representative guidance law.

Manuscript received November 4, 2004; revised March 10, 2006; released for publication December 12, 2008.

IEEE Log No. T-AES/45/1/931999.

Refereeing of this contribution was handled by T. F. Roome.

This research was funded under the JPL Mars Technology Program.

Authors' address: NASA–Jet Propulsion Laboratory, California Institute of Technology, 4800 Oak Grove Dr., Pasadena, CA 91109-8099, E-mail: (scott.r.ploen@jpl.nasa.gov).

I. INTRODUCTION

The safety of potential landing sites is without question the single most important factor in NASA landed exploration missions, for the simple reason that there will be no science return if the spacecraft does not land safely. The current practice for safe landing site selection on Mars is based on human visual examination of prior aerial images of candidate landing sites obtained by orbiters. For example, in the Mars Exploration Rover (MER) mission, the landing site selection process was driven by science return and safety constraints. Mars surface data was extracted from Mars orbiter camera (MOC) and thermal emission imaging system (THEMIS) images obtained by the Mars Global Surveyor (MGS) and Mars Odyssey missions. Mars scientists selected 185 potential sites of science interest, but only four of them satisfied safety constraints, two of which were chosen for the mission. In all NASA landed missions thus far, once the landing site is selected, the spacecraft performs a blind landing operation with no provision for corrective maneuvers prior to touchdown. This approach would be satisfactory if precise landing accuracy of the spacecraft and accurate prior knowledge of the landing site characteristics could be achieved. However, these requirements are not met in practice, and consequently the mission designers have to select a large, safe, but scientifically less interesting site for spacecraft landing.

In a current research and technology development task at JPL, we are developing a novel capability for on-board, real-time assessment and avoidance of terrain hazards while the spacecraft is descending toward the surface. This is performed using multiple active and passive sensors on-board the spacecraft. As a result, if the original site is found to be unsafe, the spacecraft can use this information to perform lateral maneuvers to avoid terrain hazards and land in a safe site. Hence, the spacecraft does not rely solely on a priori aerial site images for safe landing.

An important factor to be considered in this process is the fuel requirement for the spacecraft to retarget. Specifically, the ability to compute an estimate of the landing footprint is critical as any proposed safe landing site must be commensurate with the control authority of the spacecraft. In other words, a landing site deemed safe by on-board analysis of the terrain map will become a viable candidate landing site only if it lies within the reachable landing footprint of the spacecraft. Here the landing footprint is defined as the area on the surface of the planet that the spacecraft can reach during powered descent with a given amount of fuel. The deterministic elliptical landing footprint derived in this paper should not be confused with the statistical landing area dispersion ellipse associated with a spacecraft during Mars entry and descent.

The landing footprint is primarily dictated by the amount of fuel necessary to realize a soft landing. The ability to provide an on-board estimate of the landing footprint is an integral part of an autonomous terminal hazard avoidance system. Moreover, once knowledge of the reachable landing area has been obtained, it is desirable to assess the quality of each candidate landing site. For example, given two candidate landing sites deemed equally safe by on-board analysis of the terrain map, it is reasonable to expect that the best landing site is the one that can be attained with minimum fuel consumption.

It is also critical to have the ability to quantify the safeness of each feasible landing site in a computationally efficient manner before a decision can be made about where the vehicle should land. To this end, a fuzzy-logic-based autonomous reasoning engine is developed to fuse sensor data along with knowledge of the landing footprint to enable the spacecraft to make an on-board autonomous choice of the landing site [2]. This on-board capability is critical as it will enable the spacecraft to autonomously distinguish between a set of candidate landing sites that lie within close range of one another. For example, if the best landing site is isolated, it may be preferable from a hazard avoidance perspective to choose a slightly suboptimal site that is proximate to other candidate landing sites.

In this paper, we focus on a proposed spacecraft landing scenario beginning at an altitude of about 10 km with a lander attached to a subsonic parachute. The terminal descent phase of a representative Mars landing scenario is shown in Fig. 1. The subsonic parachute is jettisoned at an altitude between 500–1000 m when the spacecraft has reached a terminal vertical velocity of approximately -50 m/s. At this altitude, the powered terminal descent phase is initiated during which the spacecraft is actively controlled to a safe landing site on the surface of the planet. During both the parachute and the powered terminal descent phases, on-board sensors such as LIDAR[1] and phase-array radar will construct a real-time terrain map of the approaching surface. This topographic map will provide on-board information regarding the safeness of potential landing sites. The metric used for quantifying safeness of a landing area involves local surface roughness, slope, density of large rocks, and so on, and is discussed later in the paper.

A major contribution of this paper is the development of an efficient algorithm based on a ballistic analysis to estimate the reachable landing area available to a spacecraft during the terminal descent phase of a soft landing. The goal is to be able to generate a real-time estimate of the landing footprint for use in an on-board hazard detection and avoidance system. Our results are novel in that the landing area can be estimated quickly without requiring the use of a complex guidance law. To assess the accuracy of the landing area predictor, we compare the size of the ballistic-based landing footprint to the footprint resulting from directly integrating a representative guidance law [1, 4]. Next we describe a novel on-board fuzzy-logic-based inference engine. We discuss the metric used to quantify landing site safeness and discuss how it incorporates the landing area estimate. As will be shown, any differences arising between the ballistic-based and guidance-law-based landing footprints can be easily incorporated within the fuzzy-logic framework.

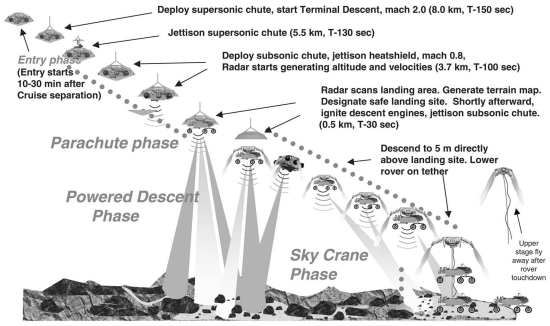

Fig. 1. Timeline for proposed Mars terminal descent.

II. ESTIMATION OF THE LANDING FOOTPRINT

In this section, the goal is to develop an algorithm to estimate the reachable landing area associated with a spacecraft during the terminal (i.e., post-parachute) landing phase of a planatery soft landing.

Although the analysis presented below focuses on the terminal landing phase, the landing footprint can also be predicted during the subsonic parachute phase (altitudes > 1 km) by integrating an on-board spacecraft/parachute model forward in time until the parachute is jettisoned. This scheme allows us to predict where the lander will be at parachute separation and allows us to predict the landing footprint at the initiation of the controlled terminal descent phase. Information about the predicted landing area during the parachute phase is particularly valuable as it allows on-board sensors to concentrate on the region where the vehicle will have the highest probability of landing. During this period, on-board algorithms will characterize the safeness of feasible landing sites and produce a safeness-ranked listing of feasible landing sites. Once the parachute is jettisoned, and control authority is regained, the spacecraft is steered to the best landing site as determined during the parachute phase. During terminal descent, the

[1]The LIDAR sensor provides range data that can be converted into an elevation map for extracting terrain characteristics such as slope and roughness.

spacecraft will continue to process sensor information regarding the local terrain and it will have the capability to autonomously retarget to a safer location if necessary.

In order to develop a landing area predictor for on-board use, we make a number of simplifying assumptions as follows.

A1: The spacecraft is modeled as a point mass during the terminal descent phase. Further, the mass of the spacecraft does not vary over terminal descent.

A2: The local gravity vector is constant.

A3: The rotation of the planet is ignored over the time in which the terminal descent phase occurs (20–30 s). As a result, the planatery surface-fixed frame (PSF) serves as an approximate inertial frame for the analysis.

A4: The spacecraft thrusters can exert an ideal impulse in any direction, thus providing an instantaneous change of the spacecraft velocity vector (i.e., instantaneous ΔV).

A5: Only a finite amount of ΔV is available for the terminal descent phase. The total amount of ΔV allocated, denoted by ΔV_a, provides a direct measure of the mass of propellant required to realize a soft landing via the rocket equation [6]

$$\Delta V_a = -g_e I_{sp} \ln\left(\frac{m_0}{m}\right). \tag{1}$$

Here g_e denotes the magnitude of local gravity vector on Earth, I_{sp} denotes the specific impulse of the thrusters, m_0 is the mass of the vehicle prior to the burn, and m is the mass of the spacecraft after the burn.

A6: All nongravitational environmental effects such as atmospheric drag and wind disturbances are neglected during the terminal descent phase.

A7: Variations in the planatery surface elevation are neglected for the landing area calculation.

It is important to emphasize that the above assumptions are not representative of the actual spacecraft (e.g, the actual spacecraft has nonnegligible attitude dynamics, cannot provide instantaneous thrust, has varying mass due to expelled propellant, and so on). These assumptions are idealizations for developing a model that leads to an explicit closed-form landing area prediction for on-board computation. In-so-far as the actual spacecraft landing footprint differs from that predicted under these ideal assumptions, the fuzzy logic rule-base can be tuned to account for any discrepancy. For example, if the ballistic-based estimate of the footprint overpredicts the actual landing footprint, landing sites near the footprint boundary are excluded as potential targets.

We now apply the theory of ballistics to estimate the landing footprint. Specifically, we assume that

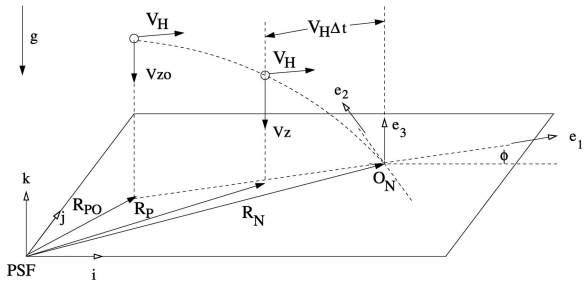

Fig. 2. Nominal ballistic trajectory.

the nominal trajectory of the spacecraft is a ballistic (free-fall) trajectory as shown in Fig. 2. The terminal point of the nominal ballistic trajectory, denoted by 0_N, is the nominal landing site. This idealized terminal descent scenario is justified under the assumption that the descent thrusters can provide instantaneous changes in the spacecraft velocity. As a result, we assume that the lander remains in free-fall until it is directly over the desired landing site. At the instant before impact, the total accumulated velocity vector is nulled by commanding the appropriate thrust vector required to realize a soft landing.[2] This situation is an approximation of the actual scenario (i.e., where the vehicle follows a controlled guidance generated trajectory) that allows an analytical solution to be obtained for the landing footprint. Later in the paper, we will compare the size of the landing area obtained via a ballistic analysis to the landing area predicted by the guidance equations.

Fig. 2 provides a detailed illustration of the idealized terminal landing scenario. In order to describe the motion of the spacecraft relative to the surface of the planet, we introduce a PSF $\mathcal{F}_{\text{PSF}} = [\vec{i}, \vec{j}, \vec{k}]$ located at a specified point on the surface. It follows from neglecting the rotation of the planet that $\mathcal{F}_{\text{PSF}}$ provides an approximate inertial frame of reference.

The nominal trajectory of the lander is assumed to be ballistic; as a result, the motion of the system is described by the standard equations

$$\vec{a} = -g\vec{k} \tag{2}$$

where g denotes the magnitude of the local gravity vector. Integrating (2), and resolving in $\mathcal{F}_{\text{PSF}}$, yields

$$v(t) = \begin{bmatrix} v_{x0} \\ v_{y0} \\ v_{z0} - gt \end{bmatrix} \tag{3}$$

where $v_0 = [v_{x0} \;\; v_{y0} \;\; v_{z0}]^T$ is the velocity of the spacecraft at the initialization of terminal descent. It can be seen from Fig. 2 that the nominal motion of the lander takes place in a plane determined by its

[2]Here we assume that the nominal ballistic trajectory has been initialized so that sufficient fuel is available to realize a soft landing at the nominal target.

resultant horizontal velocity vector $\vec{v}_H$ and the vertical velocity vector $\vec{v}_z$. As a result,

$$v(t) = v_H + v_z(t) \tag{4}$$

where $v_H = [v_{x0}\ \ v_{y0}\ \ 0]^T$ and $v_z(t) = [0\ \ 0\ \ v_{z0} - gt]^T$.

The geometry of the nominal trajectory is shown in Fig. 2. The direction determined by the horizontal velocity vector $\vec{v}_H$ is the (nominal) down-range and is denoted by the unit vector $\vec{e}_1$. The down-range direction makes an angle of $\phi = \arctan 2(v_{y0}, v_{x0})$ relative to the x-axis of $\mathcal{F}_{\text{PSF}}$ where $\arctan 2(\cdot,\cdot)$ denotes the four-quadrant arctangent function. It can be shown that the horizontal velocity vector can be expressed in terms of the down-range as follows

$$\vec{v}_H = v_H \vec{e}_1 \tag{5}$$

where $v_H = \sqrt{v_{x0}^2 + v_{y0}^2}$ is the magnitude of $\vec{v}_H$ and $\vec{e}_1 = \cos(\phi)\vec{i} + \sin(\phi)\vec{j}$. The direction orthogonal to the nominal down-range is the nominal cross-range and is given by the unit vector $\vec{e}_2$. Here $\vec{e}_2$ is chosen to complete the right-handed triad associated with $\vec{e}_1$ and $\vec{e}_3 = \vec{k}$.

Integrating (2) a second time and expressing the results in $\mathcal{F}_{\text{PSF}}$ yields

$$r(t) = \begin{bmatrix} x(t) \\ y(t) \\ z(t) \end{bmatrix} = \begin{bmatrix} x_0 + v_{x0}t \\ y_0 + v_{y0}t \\ z_0 + v_{z0}t - \frac{1}{2}gt^2 \end{bmatrix} \tag{6}$$

where $r_0 = [x_0\ \ y_0\ \ z_0]^T$ denotes the initial position of the lander at the beginning of the terminal descent phase.

The time taken for the spacecraft to impact the surface along its nominal ballistic trajectory is found by setting $z = 0$ in (6) yielding $t_{\text{go}} = (v_{z0} + \sqrt{v_{z0}^2 + 2gz_0})/g$. The nominal landing site R_N is given by

$$R_N = \begin{bmatrix} x_N \\ y_N \\ z_N \end{bmatrix} = \begin{bmatrix} x_0 + v_{x0}t_{\text{go}} \\ y_0 + v_{y0}t_{\text{go}} \\ 0 \end{bmatrix}. \tag{7}$$

Another expression for the nominal landing site relative to the origin of $\mathcal{F}_{\text{PSF}}$ is given by

$$\vec{R}_N = \vec{R}_P(t) + (v_H \Delta t)\vec{e}_1 \tag{8}$$

where $\vec{R}_P(t)$ denotes the instantaneous projection of the position vector on the surface of the planet and $\Delta t = t_{\text{go}} - t$. Note that multiplying the magnitude of the horizontal velocity by the time remaining until impact results in the distance to go along the down-range direction. A useful result follows from evaluating (8) at $t = 0$;

$$\vec{R}_N = \vec{R}_{P0} + \left(\sqrt{v_{x0}^2 + v_{y0}^2}\, t_{\text{go}}\right)\vec{e}_1 \tag{9}$$

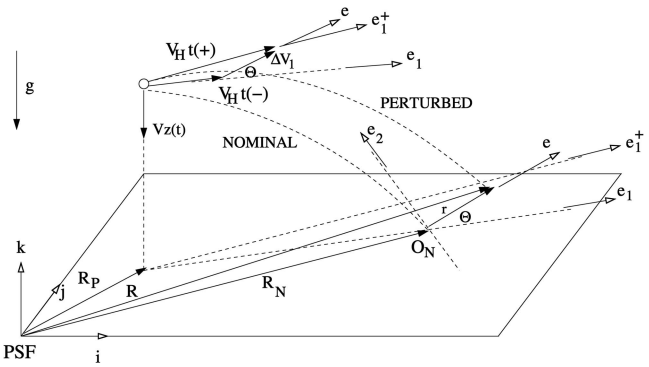

Fig. 3. Ballistic two-impulse maneuver.

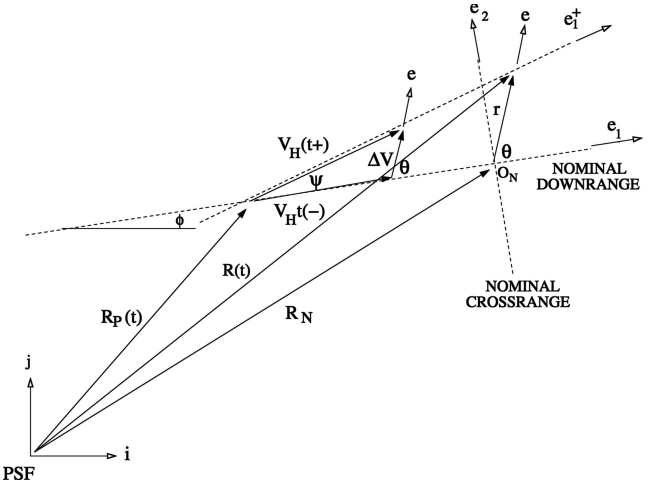

Fig. 4. Ballistic two-impulse maneuver.

where $\vec{R}_{P0}$ is the projection of $\vec{r}_0$ on the surface of the planet at the start of the terminal descent phase.

We now explain the main idea underlying the ballistic-based estimate of the landing footprint. Figs. 3 and 4 provide a pictorial representation of the method. The key is to characterize the set of ballistic trajectories at each time (centered about the nominal ballistic trajectory) that the vehicle can be made to follow while still maintaining the overall ΔV constraint. Specifically, we ask how much ΔV, say $\|\Delta\vec{V}_1\|$, can be added to the current nominal horizontal velocity vector $\vec{V}_H$ such that the vehicle still conserves enough fuel to realize a soft landing. The ΔV required for a soft landing is denoted by $\|\Delta\vec{V}_2\|$. Within the ballistic framework, a landing site is considered feasible only if there exists a ballistic trajectory connecting the current lander position to the candidate target that can be generated by a two-impulse maneuver satisfying the inequality constraint

$$\Delta V_1 + \Delta V_2 \le \Delta V_a \tag{10}$$

where $\Delta V_1 := \|\Delta\vec{V}_1\|$, $\Delta V_2 := \|\Delta\vec{V}_2\|$, and ΔV_a denotes the allocated ΔV as dictated by the amount of available propellant. The boundary of the landing footprint (i.e., the set of all feasible target sites resulting in total fuel depletion) are characterized by

the solutions of

$$\Delta V_1 + \Delta V_2 = \Delta V_a. \tag{11}$$

We now develop explicit expressions for each term in (10). Recall from (5) that $\vec{v}_H(t^-) = v_H\vec{e}_1$ where the notation t^- denotes the time immediately before the first impulse is applied. We assume that the first impulsive maneuver imparts a $\Delta\vec{V}$ of the following form

$$\Delta\vec{V}_1 = \Delta V_1\cos\theta\vec{e}_1 + \Delta V_1\sin\theta\vec{e}_2 \tag{12}$$

where $\vec{e}$ denotes the direction associated with $\Delta\vec{V}_1$ (see Fig. 3). Note that the first impulsive maneuver in the horizontal plane does not change the vertical velocity vector. Furthermore, we assume that the thrust vector can be applied in any direction in the horizontal plane.

At the instant after the first impulsive maneuver is realized, denoted by t^+, the horizontal velocity becomes

$$\vec{v}_H(t^+) = (v_H + \Delta V_1\cos\theta)\vec{e}_1 + \Delta V_1\sin\theta\vec{e}_2. \tag{13}$$

The perturbed down-range motion of the vehicle would occur in the direction determined by the unit vector $\vec{e}_1^+$ (see Figs. 3 and 4). Similarly, the total spacecraft velocity after the first impulse is realized is given by

$$\vec{v}(t^+) = (v_H + \Delta V_1\cos\theta)\vec{e}_1 + \Delta V_1\sin\theta\vec{e}_2 - v_z\vec{e}_3. \tag{14}$$

Once the resultant spacecraft velocity is known after the first impulsive maneuver has been delivered, we can immediately determine the magnitude of the second impulse required to ensure a soft landing. Specifically, it follows from conservation of energy that

$$\tfrac{1}{2}m\|\vec{v}(t^+)\|^2 + mgz(t) = \tfrac{1}{2}m\|\vec{v}(t_{\text{go}}^-)\|^2 \tag{15}$$

where t_{go}^- denotes the time immediately before impact, m is the mass of the lander, and $z(t)$ denotes the altitude of the lander at the current time.[3] The objective is to determine the magnitude of the velocity $\vec{v}(t_{\text{go}}^-)$ of the spacecraft immediately before impact. This velocity must be canceled by the second impulsive firing to ensure a soft landing. To this end, it follows from (15) that the velocity immediately before impact is

$$\|\vec{v}(t_{\text{go}}^-)\| = \sqrt{\|\vec{v}(t^+)\|^2 + 2gz}. \tag{16}$$

Substituting (14) into (16) and recalling that $v_H^2 = v_x^2 + v_y^2$, we find

$$\|\vec{v}(t_{\text{go}}^-)\| = \sqrt{\Delta V_1^2 + 2\Delta V_1 v_H\cos\theta + 2E/m}. \tag{17}$$

[3]Note that since the vertical velocity is not affected by the first maneuver, we do not distinguish between t^- and t^+ in the vertical direction.

As a result, ΔV_2 in (10) is given by

$$\Delta V_2 = \|\vec{v}(t_{\text{go}}^-)\|. \tag{18}$$

Upon substituting (12) and (17) into (10), we obtain

$$\Delta V_1 + \sqrt{\Delta V_1^2 + 2\Delta V_1 v_H\cos\theta + \frac{2E}{m}} \le \Delta V_a \tag{19}$$

where $\Delta V_1 \ge 0$. In order to determine the boundary of the reachable landing area, we seek the solution ΔV_1^* of the equation

$$\Delta V_1^* + \sqrt{\Delta V_1^{*2} + 2\Delta V_1^* v_H\cos\theta + \frac{2E}{m}} = \Delta V_a \tag{20}$$

where $\Delta V_1^* \ge 0$. After some manipulation, it follows that

$$\Delta V_1^* = \frac{\Delta V_a^2 - 2E/m}{2\Delta V_a + 2v_H\cos\theta}. \tag{21}$$

Recall that velocity is converted to range information by multiplying it by the time remaining until impact $\Delta t = t_{\text{go}} - t$. As a result, the distance to the boundary of the reachable area relative to 0_N is given by

$$r = \frac{(\Delta V_a^2 - 2E/m)\Delta t}{2\Delta V_a + 2v_H\cos\theta}. \tag{22}$$

Expressing (22) as

$$r = \frac{\dfrac{(\Delta V_a^2 - 2E/m)\Delta t}{2\Delta V_a}}{1 + \dfrac{v_H}{\Delta V_a}\cos\theta} \tag{23}$$

$$= \frac{p}{1 + e\cos\theta} \tag{24}$$

we obtain the equation of a conic section in polar coordinates where the eccentricity is

$$e = \frac{v_H}{\Delta V_a} \tag{25}$$

and the parameter of the conic is

$$p = \frac{(\Delta V_a^2 - 2E/m)\Delta t}{2\Delta V_a} \tag{26}$$

and θ denotes the polar angle. By the definition of a conic section in polar coordinates, the point from which r is measured (in this case 0_N) is a focus of the conic section. The numerical value of the eccentricity e characterizes the type of conic section represented by (23). Recalling that $\Delta V_1^* \ge 0$, it follows from (23) that

$$\Delta V_a \ge \sqrt{\frac{2E}{m}}. \tag{27}$$

We immediately find

$$\Delta V_a \ge \sqrt{v_H^2 + v_z^2 + 2gz}. \tag{28}$$

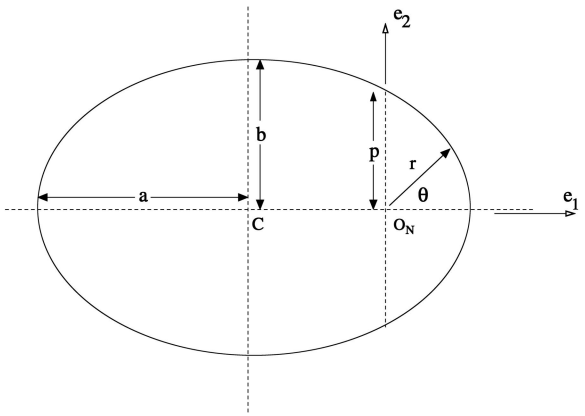

Fig. 5. Geometry of ballistic landing footprint.

Note that (28) implies that $\Delta V_a > v_H$ (this also enforces that the denominator of (23) is positive). As a result

$$e = \frac{v_H}{\Delta V_a} < 1. \tag{29}$$

Hence $0 \leq e < 1$ and it follows that the conic is an ellipse with one focus centered at the nominal landing site 0_N. The landing ellipse can also be expressed in Cartesian coordinates relative to the center C ($x = 0$, $y = 0$) of the ellipse as follows

$$\frac{x^2}{a^2} + \frac{y^2}{b^2} = 1 \tag{30}$$

where the semimajor axis is $a = p/1 - e^2$, the semiminor axis is $b = a\sqrt{1-e^2}$, and the foci are located at $x = \pm\sqrt{a^2 - b^2} = \pm ae$ and $y = 0$ (see Fig. 5). Note that in the special case of a vertical descent, $a = b$ in (30) and the landing footprint is a circle centered at point C with radius a and described by the equation $x^2 + y^2 = a^2$.

It is apparent from Fig. 5 that most of the landing footprint lies up-range of the nominal cross-range. This can be explained by noting the θ dependence of ΔV^* as exhibited in (21). We note that the magnitude of the component of $\Delta\vec{V}_1$ that can be added to $\vec{v}_H$ in the down-range direction (i.e., along $\vec{e}_1$) is limited (see Fig. 4). For example, any component of $\Delta\vec{V}_1$ in the down-range direction ($-\pi/2 < \theta < \pi/2$) increases the horizontal speed of the spacecraft. As a result, a larger terminal velocity develops and a larger fuel penalty is incurred to realize a soft landing. Conversely, if $\Delta\vec{V}_1$ has a component in the $-\vec{e}_1$ direction (i.e., $\pi/2 < \theta < 3\pi/2$) the horizontal speed is reduced and a lesser fuel penalty is incurred to realize a soft landing.

Simulations are performed to study a representative terminal landing scenario. The first simulation (Case 1) is initialized[4] at $x_0 = 0$, $y_0 = 0$ and $z_0 = 500$ m with $v_{x0} = 50$ m/s, $v_{y0} = 0$, and $v_{z0} = -50$ m/s. The value of g for Mars is 3.69 m/s^2. The resulting time evolution of the landing footprint is shown in Fig. 6. The footprint at $t = 0$ has a semimajor axis of $a = 300$ m and semiminor axis of $b = 150$ m.

An important special case occurs when $e = 0$ (i.e., $v_H = 0$). Here the spacecraft nominal trajectory is a vertical descent directly over the target and it follows that $r = p$. Recall that this represents the polar equation of a circle. As a result, the reachable landing area at any time is a circle centered at 0_N with radius $r = [(\Delta V_a^2 - 2E/m)\Delta t]/2\Delta V_a$.

[4]Here the initial conditions are commensurate with those anticipated for a future Mars lander after the subsonic parachute has been jettisoned.

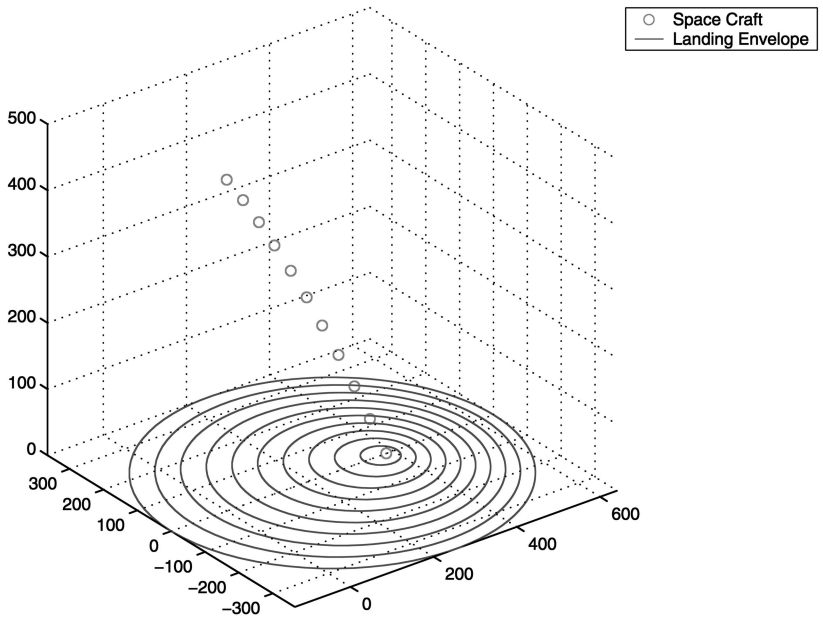

Fig. 6. Case 1—Ballistic with initial horizontal velocity.

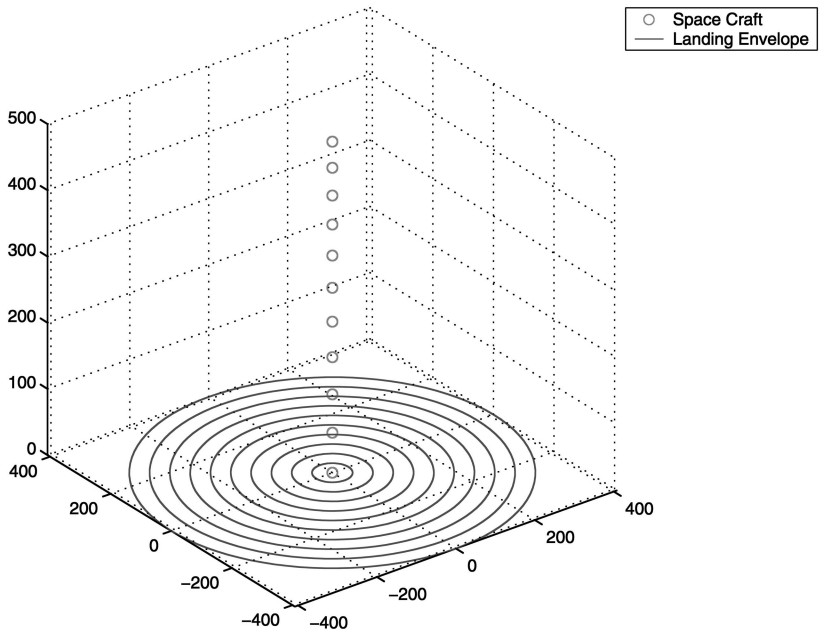

Fig. 7. Case 2—Ballistic with no horizontal velocity.

The next simulated case (Case 2) is initialized at $x_0 = 0$, $y_0 = 0$, and $z_0 = 500$ m with zero horizontal velocity (i.e., $v_{x0} = v_{y0} = 0$) and $v_{z0} = -50$ m/s. The trajectory is a vertical descent over the desired target and the resulting landing footprint is circular as shown in Fig. 7. The footprint has a maximum radius of 200 m at $t = 0$.

The distance to the boundary of the landing footprint was previously given relative to the nominal landing site 0_N. The boundary of the landing footprint relative to the origin of $\mathcal{F}_{\text{PSF}}$ is given by

$$\vec{R} = \vec{R}_N + r\vec{e} \tag{31}$$

$$= \vec{R}_{P0} + (v_H t_{\text{go}})\vec{e}_1 + r\vec{e} \tag{32}$$

where $\vec{e} = \cos\theta\vec{e}_1 + \sin\theta\vec{e}_2$ (see Fig. 3).

The ballistic equations given above are used to construct an on-board estimate of the landing footprint at any given time. The landing area calculation is performed in software during the powered terminal descent phase. At the time when the nominal landing site has been deemed unsafe, an updated target site is provided by the on-board autonomous reasoning engine.[5] The thrust vector must then be reoriented in the horizontal plane to realize the desired retargeting. We now discuss the method used to estimate the landing footprint associated with a retargeting maneuver. The new landing site $\vec{R}_N^*$ is given relative to the origin of $\mathcal{F}_{\text{PSF}}$ as

$$\vec{R}_N^* = \vec{R}_N + \vec{r}_{\text{T}} \tag{33}$$

[5]Recall that the hazard detection system will only choose feasible targets; i.e., targets that are both safe and lie within the current landing footprint. As the new target lies at an interior point of the landing footprint, it can be reached from the current state with fuel to spare.

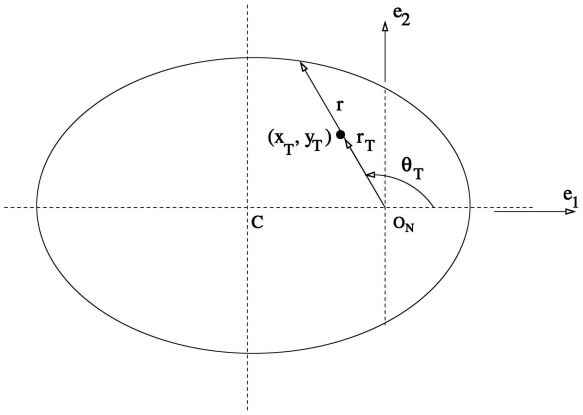

Fig. 8. Geometry of retargeting for ballistic.

where in PSF coordinates $r_{\text{T}} = R_N^* - R_N = [x_{\text{T}}, y_{\text{T}}]^T$. The thrust angle θ_{T} required for the retargeting is $\theta_{\text{T}} = \arctan 2(y_{\text{T}}, x_{\text{T}})$. The geometry of retargeting is shown in Fig. 8. The magnitude of the first impulse required, $\|\Delta\vec{V}_1\|$, is given by

$$\Delta V_1 = \frac{r_{\text{T}}}{\Delta t} \tag{34}$$

$$= \frac{\sqrt{x_{\text{T}}^2 + y_{\text{T}}^2}}{\Delta t}. \tag{35}$$

We then find

$$\Delta\vec{V}_1 = \frac{\sqrt{x_{\text{T}}^2 + y_{\text{T}}^2}}{\Delta t}(\cos\theta_{\text{T}}\vec{e}_1 + \sin\theta_{\text{T}}\vec{e}_2) \tag{36}$$

$$= \frac{\sqrt{x_{\text{T}}^2 + y_{\text{T}}^2}}{\Delta t}\vec{e}_1^+. \tag{37}$$

In order to avoid a singularity as $t \to t_{\text{go}}$ (i.e., as $\Delta t \to 0$), we require that any retargeting occur a

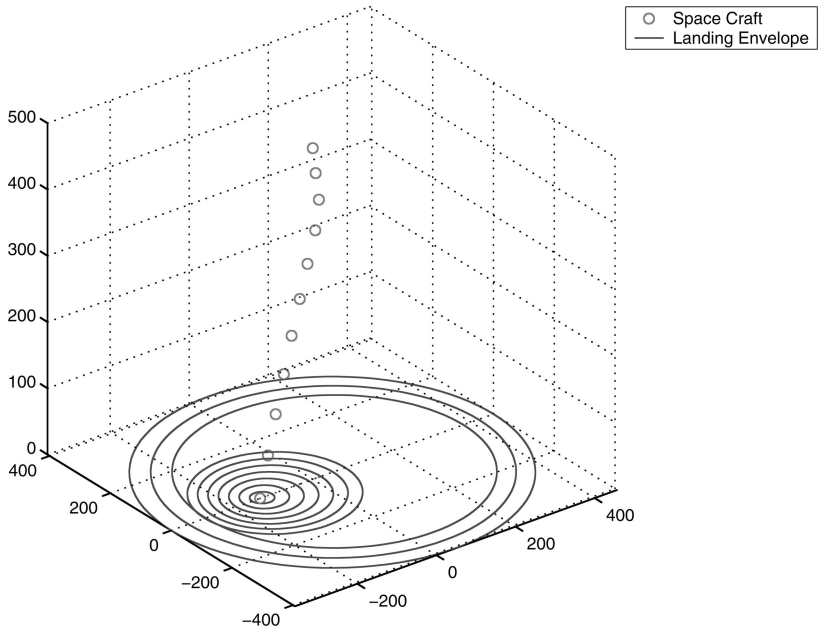

Fig. 9. Case 3—Ballistic with initial horizontal velocity and retargeting.

fixed amount of time before impact. This is not a restrictive assumption as the control authority of the vehicle becomes significantly diminished as the lander approaches the surface.

The third simulation case (Case 3) demonstrates a maneuver involving a retargeting. The lander was initialized at $x_0 = 0$, $y_0 = 0$, and $z_0 = 500$ m with $v_{x0} = 10$ m/s, $v_{y0} = 0$, and $v_{z0} = -50$ m/s. At approximately one-quarter way through the nominal landing maneuver, the on-board hazard detection system determines that the nominal target is unsafe and chooses an alternate landing site based on the safeness metric described later in this paper. The resulting time evolution of the landing footprint is shown in Fig. 9. Note the abrupt change in the trajectory (and hence the landing footprint) after the retargeting occurs.

III. DETERMINATION OF THE LANDING FOOTPRINT VIA EXPLICIT GUIDANCE LAW

In a planetary landing scenario, the spacecraft will follow a trajectory generated by an on-board guidance law during terminal descent. In this section, we determine the size of the reachable landing area obtained by integrating a representative guidance law [1, 4] and compare it with the landing area obtained via a ballistic analysis.

We assume that the terminal descent guidance law is generated by specifying a polynomial trajectory connecting the given initial state of the lander at the start of the terminal descent phase to the desired terminal state on (or near) the surface of the planet at time $t = T$. The degree of the polynomial is chosen high enough to satisfy as many terminal constraints as necessary to ensure a safe landing. Here we assume that terminal constraints are imposed on the position and velocity of the lander at touchdown, $r_{\mathrm{T}} = r(T)$ and $v_{\mathrm{T}} = v(T)$. As a result, a polynomial trajectory consisting of six unknown coefficients is required. To meet this constraint, a linear acceleration profile is specified

$$a(t) = c_0 + c_1 t \tag{38}$$

where (c_0, c_1) are unknown coefficients to be determined. It is important to note this acceleration profile represents the total acceleration (thrust + gravity) of the spacecraft. Upon integrating (38) we obtain

$$v(t) = v_0 + c_0 t + \tfrac{1}{2} c_1 t^2 \tag{39}$$

$$r(t) = r_0 + v_0 t + \tfrac{1}{2} c_0 t^2 + \tfrac{1}{6} c_1 t^3. \tag{40}$$

Substituting $r(T) = r_{\mathrm{T}}$ and $v(T) = v_{\mathrm{T}}$ into the above equations and solving for the coefficients yields

$$c_0 = -\frac{2}{T}(v_{\mathrm{T}} - v_0) + \frac{6}{T^2}(r_{\mathrm{T}} - r_0 - v_0 T) \tag{41}$$

$$c_1 = \frac{6}{T^2}(v_{\mathrm{T}} - v_0) - \frac{12}{T^3}(r_{\mathrm{T}} - r_0 - v_0 T). \tag{42}$$

In summary, the commanded acceleration profile (38) with coefficients given by (41)–(42) transfers the vehicle from (r_0, v_0) to $(r_{\mathrm{T}}, v_{\mathrm{T}})$ in time T.

We assume that a nominal landing site (x_n, y_n) on the surface has been chosen so that $r_{\mathrm{T}} = r_{nT} = (x_n, y_n, 0)$, see Fig. 10. Further we assume that $v_{\mathrm{T}} = v_{nT} = 0$ and that the initial conditions of the spacecraft at the beginning of powered terminal descent (r_0, v_0) are fixed. The nominal trajectory is then given by

$$a_n(t) = c_{0n} + c_{1n} t \tag{43}$$

$$v_n(t) = v_0 + c_{0n} t + \tfrac{1}{2} c_{1n} t^2 \tag{44}$$

$$r_n(t) = r_0 + v_0 t + \tfrac{1}{2} c_{0n} t^2 + \tfrac{1}{6} c_{1n} t^3 \tag{45}$$

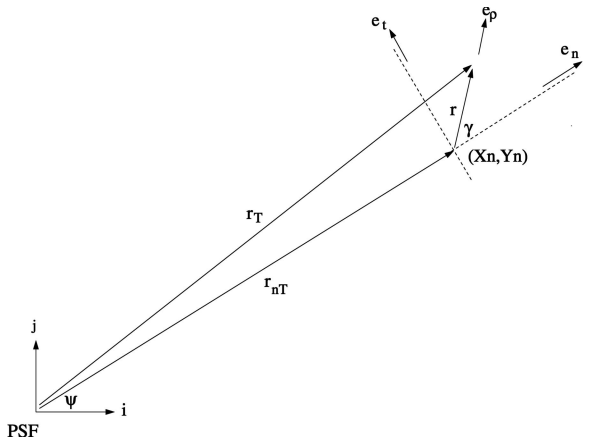

Fig. 10. Geometry of guidance-based landing footprint.

where (c_{0n}, c_{1n}) denote (c_0, c_1) in (41)–(42) evaluated at $(r_0, v_0), r_{\mathrm{T}} = r_{nT}$, and $v_{\mathrm{T}} = 0$. The acceleration profile a_n represents total acceleration of the vehicle; i.e.,

$$a_n = a_{pn} + g \tag{46}$$

where a_{pn} is the thrust acceleration delivered by the propulsion system and g is the gravity vector. Here we have neglected all other disturbance forces acting on the lander. The amount of fuel expended to reach the nominal landing site, denoted by ΔV_n, is

$$\Delta V_n = \int_0^T \sqrt{a'_{pn} a_{pn}}\, dt$$

where $'$ denotes the transpose of a matrix. The fuel capacity of the lander is assumed to be ΔV_a, where $\Delta V_a > \Delta V_n$ so that enough excess fuel is available to retarget during terminal descent if necessary.

We now discuss the computation of the landing footprint based on the linear acceleration profile given in (38). To this end, consider the geometry of the nominal target shown in Fig. 10. The position of the nominal landing site relative to the origin of PSF is denoted by $\vec{r}_{nT}$. In Fig. 10, we have introduced the unit vector $\vec{e}_n$ pointing in the direction of $\vec{r}_{nT}$, where $\vec{e}_n = \cos(\psi)\vec{i} + \sin(\psi)\vec{j}$, $\psi = \arctan(y_n, x_n)$, and $\vec{e}_t = -\sin(\psi)\vec{i} + \cos(\psi)\vec{j}$.

The boundary of the landing footprint is determined by moving the target outward from the nominal until all excess fuel available at the current time is depleted. To this end, we parameterize the target position relative to the nominal in terms of the polar coordinates (r, γ) centered at the nominal; i.e.,

$$\vec{r}_T = \vec{r}_{nT} + r\vec{e}_r \tag{47}$$

where

$$\vec{e}_r = \cos(\gamma)\vec{e}_n + \sin(\gamma)\vec{e}_t. \tag{48}$$

After some manipulation, it follows that

$$\vec{r}_T = \vec{r}_{nT} + r\cos(\psi + \gamma)\vec{i} + r\sin(\psi + \gamma)\vec{j}. \tag{49}$$

The algorithm used to determine the landing footprint is as follows.

1) Input the current time $t = t^*$.

2) Calculate the current amount of fuel remaining

$$\Delta V_a(t^*) = \Delta V_a(0) - \int_0^{t^*} \sqrt{a'_{pn} a_{pn}}\, dt.$$

3) Evaluate c_0 and c_1 in (41)–(42) at $r_0 = r_n(t^*)$, $v_0 = v_n(t^*)$, $r_T = \vec{r}_T = r_{nT} + r\cos(\psi + \gamma)\vec{i} + r\sin(\psi + \gamma)\vec{j}$, and $v_T = 0$. Denote the resulting guidance coefficients as $c_{0r}(r, \gamma)$ and $c_{1r}(r, \gamma)$.

4) Construct the total acceleration profile commensurate with the current spacecraft state and the translated target

$$a_r(t) = c_{0r}(r, \gamma) + c_{1r}(r, \gamma)t. \tag{50}$$

5) Construct the thrust acceleration required to reach the translated target

$$a_{pr} = a_r(t) - g. \tag{51}$$

6) Define

$$\Delta V(r, \gamma) = \int_{t^*}^{T - t^*} \sqrt{a'_{pr} a_{pr}}\, dt. \tag{52}$$

7) For each γ between 0 and π, search[6] for the value of r, denoted r^*, that renders

$$\Delta V(r^*, \gamma) = \Delta V_a(t^*). \tag{53}$$

8) The boundary of the landing footprint relative to the origin of PSF is then given at the current instant by

$$\vec{r}_T = \vec{r}_{nT} + r^*\cos(\psi + \gamma)\vec{i} + r^*\sin(\psi + \gamma)\vec{j} \tag{54}$$

where $r^* = r^*(\gamma)$.

9) Update $t \to t^* + \Delta t_g$ where Δt_g is the guidance update interval and repeat.

The time T allocated to reach the nominal landing site is fixed in the above algorithm. Note that the above algorithm is both iterative and computationally intensive and does not lead to a closed-form expression for the landing footprint as in the ballistic analysis.

The landing footprint associated with the guidance law is generated via numerical simulation. In the first case, the vehicle initial conditions are $r_0 = (0, 0, 500)$ m, $v_0 = (10, 10, -50)$ m/s. The time of guided flight is $T = 12$ s and $\Delta V_a = 150$ m/s. The nominal target is at the intersection of the surface with a ballistic trajectory initialized at (r_0, v_0); i.e., $r_{Tn} = (x_n, y_n, 0)$ where $x_n = x_0 + v_{x0} t_{\mathrm{go}}$ and $y_n = y_0 + v_{y0} t_{\mathrm{go}}$. The terminal velocity of the lander is assumed to be zero. The landing footprint associated with the guidance equations at $t = 0$ is shown in Fig. 11 along with the ballistic footprint based on the same initial conditions and nominal target. Note that the

[6]The landing footprint is symmetric about the $\gamma = 0$ line; as a result, only values of γ between 0 and π need be considered.

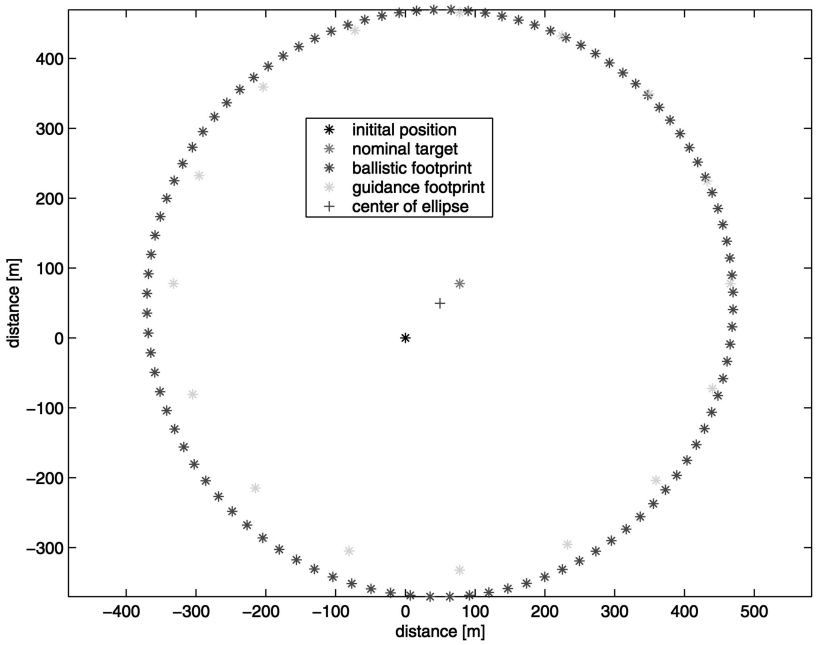

Fig. 11. Comparison of landing footprints at $t = 0$—Case 1.

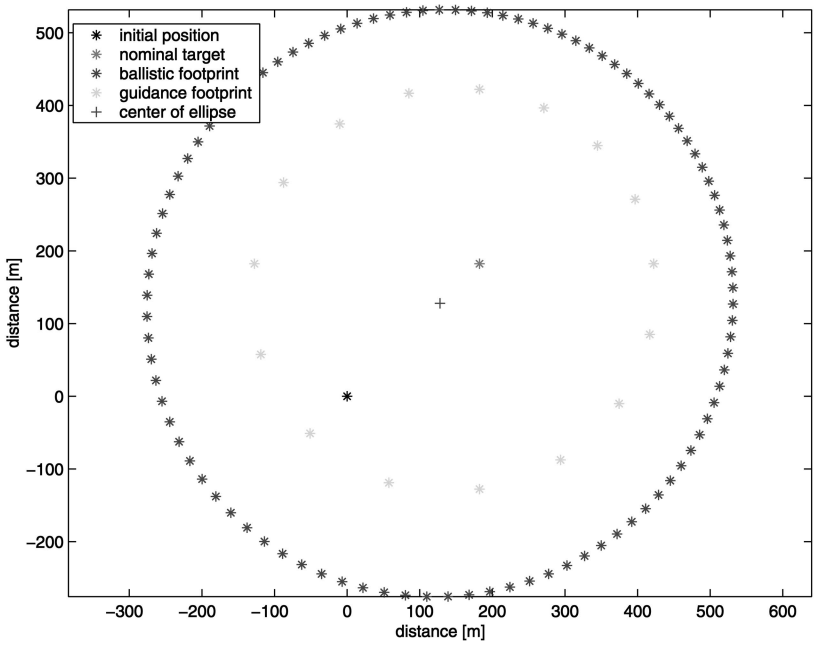

Fig. 12. Comparison of landing footprints at $t = 0$—Case 2.

ballistic footprint is in close agreement with the guidance-based landing area although it slightly overpredicts the landing area in the region lying aft of the nominal target.

For Case 2, the initial conditions are $r_0 = (0, 0, 700)$ m, and $v_0 = (20, 20, -60)$ m/s. Again the time of guided flight is $T = 12$ s with $\Delta V_a = 150$ m/s. The nominal target is chosen as the intersection of the surface with a ballistic trajectory initialized at (r_0, v_0) and the terminal velocity of the lander is again taken to be zero. The landing footprint associated with the guidance equations at $t = 0$ is shown in Fig. 12 along with the ballistic footprint based on the same initial conditions and nominal target. Note that the ballistic landing footprint overpredicts the guidance footprint by as much as 100 m in certain directions, which represents an overprediction of the landing area by approximately 50%.

After iterating over numerous initial states and times of flight T, it is observed that the ballistic-based landing footprint provides an upper-bound for the guidance-law generated landing footprint. Cases 1 and

2 above are representative examples of this behavior. The tendency of the ballistic algorithm to overpredict the landing footprint is not a major problem due to the fact that the fuzzy-logic-based landing-site quality index (described in the next section) can be tuned to penalize landing sites near the boundary of the ballistic footprint.

IV. FUZZY-LOGIC-BASED QUALITY INDEX OF THE REACHABLE LANDING AREA

In this section, we discuss a fuzzy-logic-based system for characterizing the quality of each potential landing site within the landing footprint. This work is part of an integrated effort at JPL to develop a fuzzy-logic-based autonomous reasoning engine that enables a spacecraft to continuously evaluate the terrain safety in real-time during terminal descent.

Fuzzy logic was introduced by Professor Lofti Zadeh of U. C. Berkeley four decades ago in his seminal 1965 paper [7]. Over the past 40 years, the theories of fuzzy sets and fuzzy logic have expanded significantly on the international scale. Fuzzy logic systems have found a broad range of application domains, such as: automobiles, home appliances, engineering systems, economic systems, automated reasoning and decision making systems, and expert systems. For a detailed introduction to fuzzy logic the reader should consult [3] or [5].

Fuzzy logic provides a systematic approach for representation of and reasoning with uncertain data. Data uncertainty is handled through the level of membership to predefined data sets. Each set represents a range of values of the data, and the set membership levels can take on any value in the continuous unit interval $[0.0, 1.0]$. This is in contrast to crisp sets where the membership value is either 0 or 1. Fuzzy sets have smooth and overlapping boundaries with their adjacent neighbors, so that simultaneous membership in two or more sets is allowed.

The key attributes of a fuzzy logic system are as follows.

1) Linguistic Representation: The fuzzy sets can assume linguistic variables. This provides the capability to capture a human expert's domain knowledge, intuitive reasoning, and decision-making in an expert system.

2) Uncertainty Management: Fuzzy logic provides a systemic framework for dealing with imprecise and uncertain information.

3) Simplicity: Fuzzy logic systems are implemented by a small number of simple conditional rule statements with a few inputs and outputs.

4) Extensibility: Fuzzy logic has a modular structure that makes it easy to add new modules that represent additional rules to the system.

5) Computational Efficiency: Fuzzy logic algorithms are computationally fast and efficient, and are thus strong candidates for real-time implementation.

A fuzzy-logic system is composed of the following four elements:

1) a rule-base containing a set of if-then type conditional rules containing a fuzzy logic quantification of a human expert's knowledge regarding the system of interest.

2) an inference mechanism which mimics the expert's decision-making process.

3) a fuzzification stage that converts the inputs into information that the inference mechanism can use to activate and apply rules.

4) a defuzzification stage that converts the conclusions of the inference mechanism into actual numerical values.

Fig. 13 provides a typical information flow diagram of a fuzzy-logic system for terrain safety assessment.

The goal is to determine the overall quality of each feasible landing site. To this end, we assume that landing site quality is described by the following two variables: 1) the fuel consumption f to reach the proposed site within the landing footprint, and 2) the safeness level s of the proposed site as measured by a terrain safety index. The analysis begins with numerical values of the input variables f and s associated with each terrain patch in the landing footprint. We assume that the fuel input f has been normalized so that $f \in [0.0, 1.0]$ for all feasible landing sites.[7] The safeness index s is also normalized between 0.0 and 1.0 and classifies each landing site based on terrain characteristics such as slope, roughness, density of rocks, density of craters, and so on. For a more detailed discussion of the terrain safety metric the reader should consult [2]. The output variable is the quality q of the landing site to be discussed further below.

In order to develop a quantitative measure of the overall quality q of the landing site from the independent variables f and s, each input variable is translated from a numerical variable to a linguistic variable. A linguistic variable assumes linguistic values specified by user-defined linguistic terms. Here the linguistic variables FUEL and SAFENESS are associated with their numerical counterparts fuel consumption and safeness index, respectively. The linguistic terms associated with each linguistic variable are chosen as follows

[7] Fuel consumption can be easily parameterized in terms of the ratio r_{T}/r where $r_{\mathrm{T}} = \sqrt{x_T^2 + y_T^2}$ is the distance from the point in question to 0_N and r is the distance to the landing footprint boundary from O_N along the target angle θ_{T} (see Fig. 8).

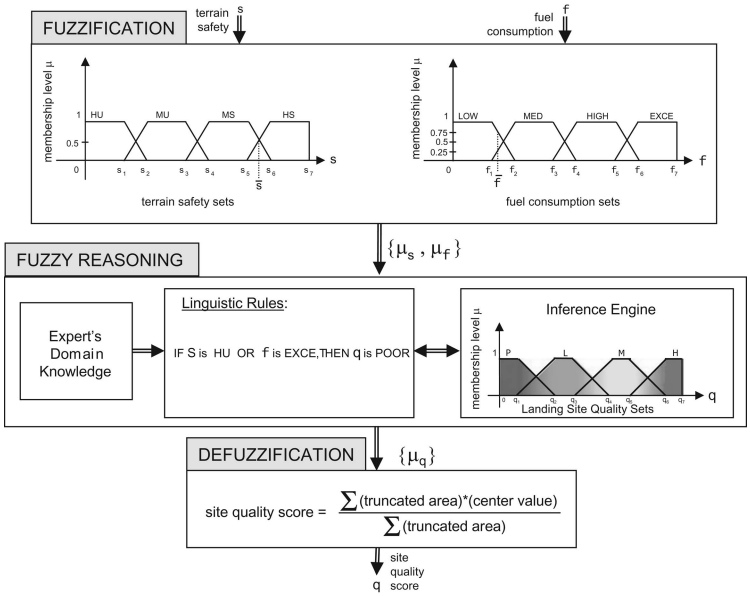

Fig. 13. Fuzzy-logic system.

(see Fig. 13):

$$\text{FUEL} = (\text{LOW, MEDIUM, HIGH, EXCESSIVE})$$

$$\text{SAFENESS} = (\text{HIGHLY-SAFE, MODERATELY-SAFE, MODERATELY-UNSAFE, HIGHLY-UNSAFE}).$$

Here each fuel class represents a band of ellipses (with foci at the nominal landing site) contained within the landing footprint at a given time. For example, sites near the boundary of the landing footprint correspond to EXCESSIVE fuel consumption, while sites close to the nominal landing site correspond to LOW fuel consumption. The quality of each feasible landing site is represented by the linguistic variable QUALITY which is described by the linguistic variables

$$\text{QUALITY} = (\text{HIGH, MEDIUM, LOW, POOR}).$$

The goal of the on-board fuzzy-logic-based reasoning engine is then to use fuzzy inference to assign a linguistic value to QUALITY for each terrain patch in the landing footprint.

The actual numerical values of the input arguments f and s are quantified using fuzzy logic by membership functions. For each input and output linguistic variable, a membership function is constructed that represents the degree to which each linguistic variable is described by a particular linguistic set. The membership function serves to define exactly what is meant by the term fuzzy set, i.e., a set S that allows grades of membership. Four membership functions are chosen for the four linguistic variables associated with the inputs f and s. The membership functions are chosen as trapezoids because they are versatile and easy to implement, although other choices are possible [5]. The membership functions allow statements such as FUEL is LOW or FUEL is MEDIUM to be quantified. Moreover, as the membership functions for adjacent linguistic sets overlap, it is possible for a given numerical value of f to be considered both LOW and MEDIUM with different degrees-of-membership simultaneously. Fig. 13 depicts for the membership functions associated with f and s, respectively.

Next, a rule base governing the linguistic variables describing the landing site selection is constructed. The rules are given in modus ponens form [5], i.e.;

- **If** *premise*, **then** *consequent*

In the terminal landing area scenario, the rules are chosen as follows:

- **If** f is LOW **and** s is HIGHLY-SAFE, **then** q is HIGH
- **If** f is LOW **and** s is MODERATELY-SAFE, **then** q is HIGH
- **If** f is LOW **and** s is MODERATELY-UNSAFE, **then** q is LOW
- **If** f is MEDIUM **and** s is HIGHLY-SAFE, **then** q is HIGH
- **If** f is MEDIUM **and** s is MODERATELY-SAFE, **then** q is MEDIUM
- **If** f is MEDIUM **and** s is MODERATELY-UNSAFE, **then** q is LOW
- **If** f is HIGH **and** s is HIGHLY-SAFE, **then** q is MEDIUM
- **If** f is HIGH **and** s is MODERATELY-SAFE, **then** q is LOW
- **If** f is HIGH **and** s is MODERATELY-UNSAFE, **then** q is POOR
- **If** f is EXCESSIVE **or** s is HIGHLY-UNSAFE, **then** q is POOR

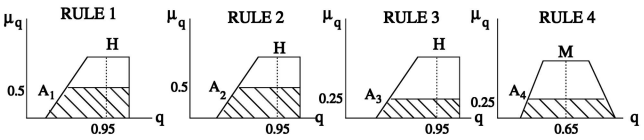

Fig. 14. Defuzzification procedure.

The fact that the ballistic landing area predictor overbounds the guidance generated landing footprint is easily incorporated in the fuzzy inference engine by forcing the QUALITY of the landing site in the above rule base to be POOR when f is EXCESSIVE. As a result, landing sites near the boundary of the footprint are automatically disqualified as viable targets.

A fuzzy inference system is required to determine which particular set of rules from the above rule set are active during the analysis of each potential landing site.[8] The inference system takes into account the recommendations from each active rule as to what linguistic value should be assigned to the quality of the site in question. This is accomplished by taking the weighted average of the truncated areas of the membership functions of the active rules associated with landing site quality (shown in Fig. 13). A defuzzification algorithm is then applied to the weighted output membership functions to produce a numerical value for the quality of the landing site. Defuzzification simply involves the computation of some measure of the area under the weighted output membership functions. Here we utilize the centroid method [5] resulting in

$$q = \frac{\sum_i b_i A_i}{\sum_i A_i} \tag{55}$$

where A_i is the truncated area of the ith output membership function, and b_i is the midpoint of the peak of the ith output membership function. Note that q is also normalized so that $0 \le q \le 1$.

To illustrate the above procedure, consider the following example. For the inputs $s = \bar{s}$ and $f = \bar{f}$ shown in Fig. 13, four rules in the above rule set are activated. The active rules, along with the membership levels for each input and output variable, are as follows:

Rule 1: **If** $\underbrace{\text{f is LOW}}_{0.75}$ **and** $\underbrace{\text{s is HS}}_{0.5}$, **then** $\underbrace{\text{q is HIGH}}_{0.5}$

Rule 2: **If** $\underbrace{\text{f is LOW}}_{0.75}$ **and** $\underbrace{\text{s is MS}}_{0.5}$, **then** $\underbrace{\text{q is HIGH}}_{0.5}$

Rule 3: **If** $\underbrace{\text{f is MED}}_{0.25}$ **and** $\underbrace{\text{s is HS}}_{0.5}$, **then** $\underbrace{\text{q is HIGH}}_{0.25}$

Rule 4: **If** $\underbrace{\text{f is MED}}_{0.25}$ **and** $\underbrace{\text{s is MS}}_{0.5}$, **then** $\underbrace{\text{q is MED}}_{0.25}$

Note that, because of the **and** operations, the membership level of the output variable q is computed as the minimum of the membership levels of the input variables. Next, the truncated area of each active membership function of q is weighted by the midpoints of the peaks of the membership functions. The truncated areas of the output membership functions are the shaded areas A_i, $i = 1,2,3,4$ shown in Fig. 14. The defuzzification process computes the centroid of the aggregate area as

$$q = \frac{0.95A_1 + 0.95A_2 + 0.95A_3 + 0.65A_4}{A_1 + A_2 + A_3 + A_4}.$$

Note that each truncated area is multiplied by the midpoint of each trapezoid peak. Utilizing the membership functions shown in Fig. 14, we find the numerical value $q = 0.871$, representing a highly desirable landing site.

Finally, the fuzzy-logic-based system is equivalent to a nonlinear input-output mapping $h(\cdot,\cdot)$; i.e., $q = h(f,s)$ where f and s are associated with each landing site within the reachable ellipse. This input-output mapping is called the control surface of the system and is shown as a 3-dimensional surface in Fig. 15.

V. CONCLUSIONS

In this paper, we develop an algorithm based on a ballistic entry analysis to estimate the landing footprint during the powered terminal descent phase of a planatery soft landing. Our approach leads to a simple analytical expression for the boundary of the landing footprint. The landing footprint generated from the ballistic analysis is then compared with the landing footprint resulting from numerically integrating a representative guidance law. Extensive simulations demonstrate that the ballistic approach overpredicts the landing footprint associated with the guidance-law-generated spacecraft trajectory. We also describe a methodology based on fuzzy logic to combine information about the landing footprint with information about the safeness of the planatery terrain to construct a landing site quality index. The landing site quality index is a critical parameter that will enable the spacecraft to make intelligent real-time decisions about landing safely on unknown and possibly hazardous planetary terrain. We argue that the ballistic-generated reachable area calculation is sufficient for designing a fuzzy-logic-based on-board inference engine for determining landing site quality. Specifically, sites near the boundary of the landing area predictor are rendered infeasible by proper selection of the fuel membership functions and formulation of the rule-base underlying the fuzzy inference engine. Further, any a priori knowledge (e.g., from off-line simulation) regarding the size of the guidance-generated landing footprint relative to the ballistic footprint can be utilized to adjust an on-board ballistic estimate of the landing area before it is provided to the inference engine.

[8] Recall that multiple rules can be active at the same time as the linguistic variables FUEL and SAFENESS are permitted to take multiple linguistic values simultaneously.

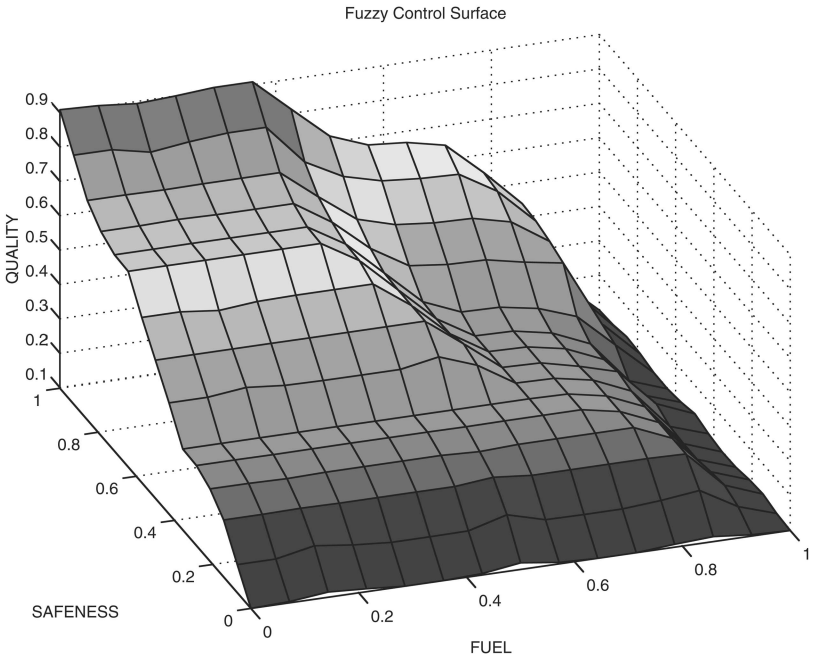

Fig. 15. Input-output control surface based on ballistics.

ACKNOWLEDGMENTS

This research was performed at the Jet Propulsion Laboratory, California Institute of Technology, under contract with the National Aeronautics and Space Administration.

REFERENCES

[1] Cherry, G. W.
E-Guidance—A general explicit, optimizing guidance law for rocket-propelled spacecraft.
MIT Instrumentation Laboratory, R-456, 1964.

[2] Howard, A., and Seraji, H.
A fuzzy rule-based safety index for landing site risk assessment.
In *Proceedings of the WAC 9th International Symposium on Robotics with Applications*, Orlando, FL, 2002.

[3] Klir, G. J., and Yuan, B.
Fuzzy Sets and Fuzzy Logic.
Upper Saddle River, New Jersey: Prentice-Hall, 1995.

[4] Klumpp, A. R.
Apollo lunar-descent guidance.
MIT Charles Stark Draper Laboratory, R-695, 1971.

[5] Passino, K. M., and Yurkovich, S.
Fuzzy Control.
Reading, MA: Addison-Wesley, 1998.

[6] Prussing, J. E., and Conway, B. A.
Orbital Mechanics.
New York: Oxford University Press, 1993.

[7] Zadeh, L. A.
Fuzzy Sets, Information and Control.
8, 3 (1965), 338–353.

Author photographs and biographies are not available.